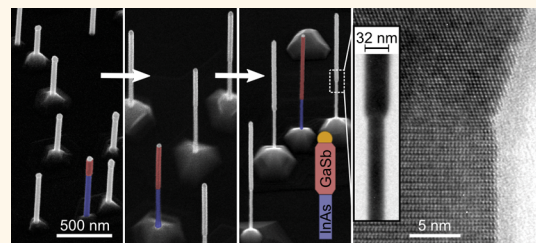


Diameter Limitation in Growth of III-Sb-Containing Nanowire Heterostructures

Martin Ek,[†] B. Mattias Borg,^{‡,§,△} Jonas Johansson,[‡] and Kimberly A. Dick^{†,‡,*}

[†]nCHREM/Polymer & Materials Chemistry, Lund University, Box 124, S-22100, Lund, Sweden, and [‡]Solid State Physics and [§]Department of Electrical and Information Technology, Lund University, Box 118, S-22100 Lund, Sweden. [△]Present address: IBM Research, Zürich, Säumerstrasse 4, CH-8803 Rüschlikon, Switzerland.

ABSTRACT The nanowire geometry offers significant advantages for exploiting the potential of III-Sb materials. Strain due to lattice mismatch is efficiently accommodated, and carrier confinement effects can be utilized in tunneling and quantum devices for which the III-Sb materials are of particular interest. It has however proven difficult to grow thin (below a few tens of nanometers), epitaxial III-Sb nanowires, as commonly no growth is observed below some critical diameter. Here we explore the processes limiting the diameter of III-Sb nanowires in a model system, in order to develop procedures to control this effect. The InAs–GaSb heterostructure system was chosen due to its great potential for tunneling devices in future low-power electronics. We find that with increasing growth temperature or precursor partial pressures, the critical diameter for GaSb growth on InAs decreases. To explain this trend we propose a model where the Gibbs–Thomson effect limits the Sb supersaturation in the catalyst particle. This understanding enabled us to further reduce the nanowire diameter down to 32 nm for GaSb grown on 21 nm InAs stems. Finally, we show that growth conditions must be carefully optimized for these small diameters, since radial growth increases for increased precursor partial pressures beyond the critical values required for nucleation.



KEYWORDS: nanowires · III–V materials · III-Sb materials · antimonides · Gibbs–Thomson · MOVPE

The III-Sb materials have many properties that are of interest for applications in electronics and opto-electronics, such as narrow direct bandgaps and high carrier mobilities, with GaSb and InSb having the highest hole and electron mobilities respectively of all III–Vs. The growth of these materials as epitaxial nanowires has been accomplished by metalorganic vapor phase epitaxy (MOVPE) for GaSb^{1–3} and InSb.^{4–7} For the latter chemical beam epitaxy (CBE)^{8,9} and molecular beam epitaxy (MBE)¹⁰ have also been used. Epitaxial nanowires of the III-Sb ternary InGaSb,¹¹ as well as various other Sb containing ternaries such as GaAsSb,^{12,13} InAsSb,^{10,14,15} and InPSb¹⁶ have also been reported. The nanowire morphology is particularly advantageous for heterostructures containing these materials, as it is able to accommodate lattice mismatch (caused by the large lattice parameters of the III-Sb materials) to a greater extent than thin films.¹⁷

In addition to reduced formation of misfit dislocations at heterointerfaces, the thin

nanowire geometry can provide further benefits for some of the applications for InSb and GaSb. Thin InSb nanowires are one platform proposed for the creation and detection of Majorana fermions, and have recently been used to produce signatures thereof for the first time.^{18,19} GaSb combined in a heterostructure with InAs has potential for tunneling devices, where a small diameter would reduce carrier thermalization and improve performance by more ideal gate coupling and less scattering.^{20,21} In addition, GaSb nanowires are of interest for single hole transistors, with applications in spintronics.²²

Very thin III-Sb nanowires have been synthesized by vapor transport chemical vapor deposition methods, with diameters down to 5 nm for InSb^{23,24} and 20 nm for GaSb.²⁵ These methods however do not easily offer the possibility of creating heterostructures or adding dopants, and generally do not result in epitaxial nanowires (with exceptions reported for thicker nanowires^{26,27}). Using the alternative MOVPE,

* Address correspondence to kimberly.dick@ftf.lth.se.

Received for review February 8, 2013 and accepted March 6, 2013.

Published online March 06, 2013
10.1021/nn400684p

© 2013 American Chemical Society

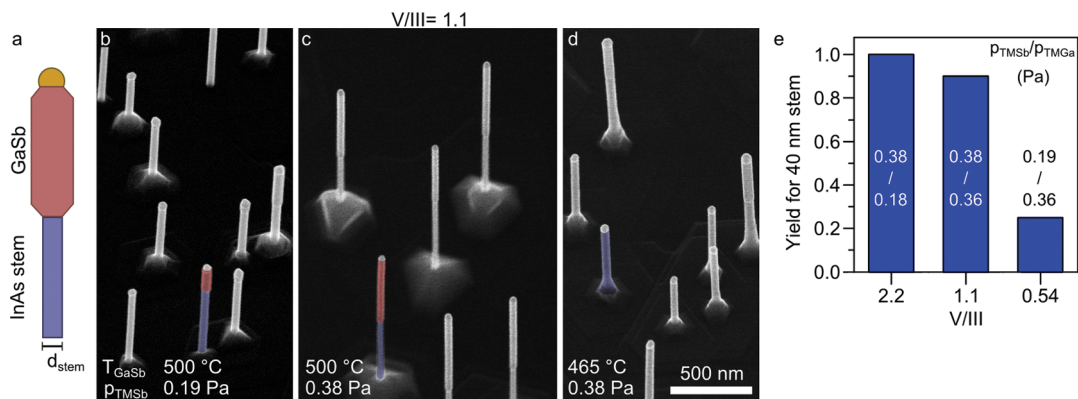


Figure 1. (a) Schematic of the InAs–GaSb nanowires. (b–d) SEM images recorded at 30° tilt of nanowires grown from nominally 30–70 nm gold particles, all at V/III = 1.1. (c) Reference sample grown with $T_{\text{GaSb}} = 500 \text{ }^{\circ}\text{C}$ and $p_{\text{TMSb}} = 0.38 \text{ Pa}$. (b, d) Nanowires grown at a lower p_{TMSb} and T_{GaSb} , respectively. Note that all nanowires in panel c contain a GaSb segment (colored according to the schematic for one nanowire in each image), while only a few in panels b and d do. (e) Yield for 40 nm stems at varying V/III ratio (series C).

CBE, and MBE methods on the other hand has proven difficult in the growth of III–Sb nanowires from small diameter catalyst particles, as noted in earlier reports.^{4,28} In addition the III–Sb nanowires will generally have larger diameters than the corresponding III–As or III–P nanowires, further limiting the minimum attainable diameter, for two reasons. In both gold- and self-catalyzed growth, III–Sb nanowires will generally have larger diameters than the corresponding III–As or III–P, since III–Sb materials are generally grown from catalyst particles with significantly higher concentrations of group III^{2,4} and possibly group V atoms.^{5,6} Sb can also strongly increase the radial growth, even for small local variations in the V/III ratio.⁷ This makes it desirable to initiate growth from as small diameter particles as possible.

In this study we investigate the effect of the seed particle diameter on the growth of III–Sb material for the technologically interesting InAs–GaSb heterostructure. In the reverse growth direction (GaSb–InAs) such nanowires have shown excellent tunneling properties,^{21,29} but always form $\text{InAs}_{1-x}\text{Sb}_x$ rather than pure InAs due to Sb carry-over. Because of the Sb content this segment necessarily adopts the zincblende crystal structure type and has a narrow band gap, which may be unwanted for some applications.³⁰ These constraints are both avoided for the InAs–GaSb growth direction studied in this report. Here, previous reports instead indicate that a minimum 25 nm long nominal GaAs insert is needed to facilitate proper nucleation of the GaSb segment on the InAs stem, which could reduce tunneling performance by acting as a barrier.³¹ We show here that by tuning the temperature and precursor partial pressures at the materials switch, it is possible to grow InAs–GaSb heterostructures without the intentional growth of a GaAs segment between the two materials. The resulting nanowire growths display a clear diameter dependence: the nucleation of the GaSb segment usually fails for the thinnest

nanowires, below some critical diameter. In this report we explore the diameter limitation in this system using a growth model³² which includes the Gibbs–Thomson effect (previously used for studying the diameter-dependent growth rate in InGaSb¹¹ and InAs³³) acting on Sb.

RESULTS AND DISCUSSION

A schematic of the InAs–GaSb nanowire heterostructure is shown in Figure 1a. In the following presentation and discussion of the results the GaSb growth temperature is denoted T_{GaSb} and the partial pressures of the precursors is given as the trimethyl-antimony (TMSb) partial pressure, p_{TMSb} , at a constant V/III of 1.1 (unless otherwise noted). Figure 1 panels b and c show scanning electron microscopy (SEM) images recorded of samples with GaSb grown at $T_{\text{GaSb}} = 500 \text{ }^{\circ}\text{C}$ but with different precursor partial pressures (p_{TMSb} of 0.19 and 0.38 Pa, respectively). The conditions used for the sample in panel c will be used as a reference throughout this report. For the purpose of calculating yield in this report we have considered as failed those nanowires consisting only of InAs, while all nanowires containing a GaSb segment, independent of its length, were considered successful. The presence of this segment was readily visible by SEM due to an expansion of the nanowire diameter, which is characteristic of III–Sb growth in Au seeded nanowires.^{1,2,4,34} Typical morphologies for successful and failed nanowires are shown in Figure 1b–d. We have confirmed by transmission electron microscopy (TEM) and energy dispersive X-ray spectroscopy (EDX) that for these growths the wider top segment is uniquely associated with the presence of GaSb. The lower precursor partial pressures resulted in a low yield of GaSb segments on top of the InAs stems, with consistently successful growth only for nanowires with a stem diameter of 70 nm or larger. For the higher precursor partial pressures sample the yield increased

to 100% for nanowires with stem diameters of 50 nm and larger. A similar trend as for increasing p_{TMGa} can also be seen with increasing T_{GaSb} , as illustrated by the SEM images in Figure 1 panels c and d which were recorded of samples grown with the same p_{TMGa} , but at different T_{GaSb} (500 and 465 °C, respectively). The diameter dependence of the yield will be the main focus of this report and is analyzed separately in the coming sections.

It is apparent from Figure 1b,c that the nucleation of the GaSb section on the InAs stem is limited by the flow of precursor material. To determine whether the nucleation is limited by the supply of Ga or Sb, the partial pressure of each precursor was reduced to half of that in the reference procedure while keeping the other constant (series C, see Methods). Figure 1e shows the resulting yield of nanowires with stem diameters of 40 nm for these growths together with the reference nanowires. The reduction in p_{TMGa} (V/III=2.1) did not adversely affect the GaSb yield, apparently even resulting in a small improvement compared to the standard procedure. The reduction of p_{TMGa} (V/III=0.54) on the other hand dramatically reduced the yield, implying that the nucleation is group V limited. This trend in yield with changing V/III is present also for other stem diameters.

The composition of the gold particle was measured by EDX after 45 min of GaSb growth. A clear difference could be seen between the nanowires which successfully nucleated GaSb and those which stopped growing after forming the InAs stem. While the particles in both cases contained roughly 50 atom % group III (Ga + In), the successfully grown nanowires had 5 atom % In, while the failed had 12 atom % In. To determine whether the difference in group III content could be responsible for the success or failure of nucleating GaSb we investigated a sample where the GaSb growth was terminated after 5 min (see Figure 2), but otherwise followed the reference procedure. In this case no difference could be measured between the nanowires, all having approximately 34 atom % Ga and 21 atom % In in the gold particle. A significant expulsion of material during cool-down is unlikely as no neck region or segment with a different composition underneath the gold particle was observed. This strongly indicates that there is no difference in group III content in the catalyst particle at the beginning of the GaSb growth which could affect the nucleation. The difference seen after the long GaSb growth times is instead likely caused by the growth of the GaSb segment, during which In from the particle can be incorporated in the nanowire, thus reducing the amount remaining in the catalyst particle. Sb was found in all gold particles in the range of 1–2 atom %. However, the combination of low concentrations and peak overlap with In makes the Sb quantification uncertain, precluding any comparison between failed and successful nanowires.

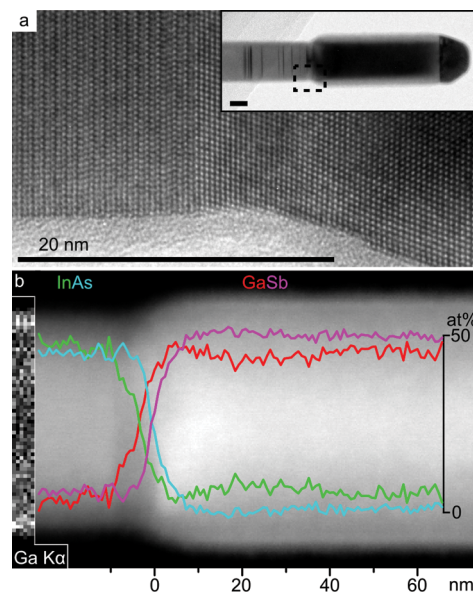


Figure 2. (a) HRTEM image of the InAs/GaSb heterojunction in a nanowire grown using the reference procedure, but with only 5 min GaSb growth time. The image was recorded in $<1-10>$ and shows the transition from wurtzite InAs to zincblende GaSb. The inset shows an overview image of the nanowire. The scale bar is 20 nm in both cases. (b) HAADF-STEM image of the heterojunction area with an overlaid EDX profile. The group III switch starts slightly before the group V switch, both occurring over approximately 12 nm. The inset on the left is a Ga $\text{K}\alpha$ map from the InAs stem, showing a thin GaSb shell.

The heterostructures resulting from the reference procedure were further investigated by TEM, using the sample with 5 min GaSb growth in order to keep the overgrowth of the heterojunction area to a minimum. Figure 2a shows a high resolution TEM (HRTEM) image of the heterojunction area, with wurtzite InAs and zincblende GaSb. Figure 2b shows a high angle annular dark-field (HAADF) scanning TEM (STEM) image of the same area overlaid with an EDX line profile. The HAADF image shows a short (approximately 10 nm) segment with dark contrast between the InAs stem and the GaSb segment. According to the EDX line scan this segment contains graded $\text{In}_{1-x}\text{Ga}_x\text{As}$ with $x = 0-0.5$ in the first half, continuing into the second half which also contains increasing quantities of Sb as the group V switch commences. Because of the short length and graded composition of this segment, the accuracy of the EDX quantification is low as some of the surrounding material is likely also included in the analysis. A comparison of the (111) plane spacing in the growth direction reveals a contraction of a maximum 4% compared to the InAs, which corroborates the EDX quantification by indicating a composition of approximately $\text{Ga}_{0.6}\text{In}_{0.4}\text{As}$, provided that the segment is unstrained in the axial direction. This assumption is validated by strain measurements on nanowires with abrupt compositional changes, which show that the axial strain is relaxed very efficiently.³⁵ There is also

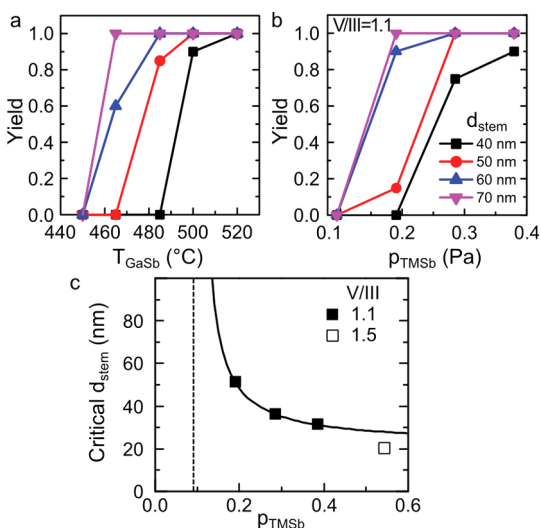


Figure 3. (a) Diameter-dependent yield of GaSb segments as a function of GaSb growth temperatures (series A). (b) Diameter-dependent yield as a function of TMSb partial pressure at constant V/III ratio (series B). For clarity only four diameter cohorts are shown. (c) Plot of the smallest diameters for which GaSb growth was successful as a function of p_{TMSb} measured from series A. The dashed vertical line represents the $p_{\text{TMSb}} = 0.095$ Pa sample, in which no GaSb growth was observed for any diameter. The best fit for the Gibbs–Thompson model is also included, showing good agreement with the measurements. The open square represents the highest TMSb partial pressure, grown using a higher V/III ratio (sample E).

some In carryover into the GaSb segment evident from EDX, resulting in $\text{Ga}_{0.9}\text{In}_{0.1}\text{Sb}$ immediately after the switch, but with a rapidly decreasing In content away from the heterojunction. Despite the compositional changes across the interface no misfit dislocations could be seen in the HRTEM images. The EDX map inset in Figure 2b shows the presence of a GaSb shell on the InAs stem, also evident from the apparent nonzero Ga content in the InAs segment from the line scan. This shell is too thin to be accurately measured from these images, but is estimated to about 1 nm from EDX quantifications of the InAs segment. Although quite thin, this shell consists of wurtzite GaSb which to our knowledge has not been reported previously.

Diameter Dependence. We next analyzed samples with systematically varied GaSb growth temperatures and precursor partial pressures for a range of diameter (series A and B, see Methods). By grouping the nanowires according to the diameter of their InAs stems (using 5 nm cohorts, as described in the Materials and Methods section) we could observe a clear diameter dependence for the GaSb yield. Figure 3 panels a and b, respectively, show the increase in yield with GaSb growth temperature and total precursor partial pressures (constant V/III = 1.1), for four distinct stem diameter cohorts. The measured stem diameters include the GaSb shell, but due to its limited thickness this should not distort the trends presented here. For any given diameter the probability of successfully

nucleating, and subsequently growing, a GaSb segment is close to zero at low GaSb growth temperatures or precursor partial pressures. The yield then increases rapidly once a certain minimum T_{GaSb} or p_{TMSb} is reached. The temperature or flow where this dramatic increase in GaSb yield occurs is shifted toward higher T_{GaSb} and p_{TMSb} with decreasing diameters, indicating that the underlying effect is strongly diameter dependent. It is worth noting that although a high yield was eventually reached for all diameters included in Figure 3, the 30 nm and below stems also present in these samples did not nucleate GaSb segments with any considerable yield under any of these conditions.

As the GaSb nucleation was limited by Sb, the minimum total precursor partial pressure described above can be interpreted more specifically as a minimum Sb partial pressure. The diameter dependence of this minimum Sb partial pressure can equivalently be stated as there being a critical diameter, below which no GaSb nucleates, which depends on the Sb partial pressure. In this case the yield should rapidly fall to zero for diameters smaller than the critical diameter and quickly increase to one for larger diameters, which describes the observations from the growth series well. For some diameters there do seem to be partial pressures where the yield is high, but not 100% (60 and 40 nm) or low, but not 0% (50 nm). However this can be explained by the critical diameter specified by the Sb partial pressure falling somewhere inside the diameter cohort, which will then contain nanowires both somewhat larger and smaller than the critical diameter.

The explanation for the equally clear trend in yield with temperature is more difficult to identify, as increasing the temperature will have multiple effects on the growth. However we note that the decomposition rates of TMGa (trimethylgallium) and TMSb are temperature dependent. Since the growth is performed in a constant flow system where the precursors have a short residence time, the amount of decomposed precursor material available for growth will depend directly on the decomposition rate. One of the effects of an increased temperature would therefore be to increase the amount of Sb (and also Ga) available for growth. For planar GaSb growth using these precursors the growth rate has been shown to depend exponentially on temperature up to 575 °C,³⁶ supporting a temperature effect on the precursor availability throughout the temperature interval used in the growths reported here. Thus the increased yield with temperature in this interval can, at least partially, be explained by the same mechanism as the increase with precursor partial pressures.

The InAs stems grew longer with smaller diameters, which can be explained by a surface diffusion limited growth rate.³³ The increased stem length could potentially adversely affect the GaSb growth by limiting the

supply of precursors from surface diffusion. To preclude this effect we investigated samples with varying stem lengths by varying the InAs growth time for otherwise identical conditions (series D). A small decrease in GaSb yield was observed for the very longest (several μm) stems, but for the stem lengths typically used for the samples in this study the stem length effect is negligible compared to the diameter effect. In growths under similar conditions the Sb surface diffusion length was estimated to 50 nm.¹¹ Since the InAs stems are always much longer than this we do not expect to see any effects due to a limitation in the amount of Sb supplied from surface diffusion for the longer stems.

Gibbs–Thomson Model. Having discounted a limitation of available Sb due to diameter-dependent stem lengths, we instead investigate a size-dependent limitation of the Sb supersaturation in the alloy particle due to the Gibbs–Thomson effect. An increase in vapor pressure of Sb in the alloy particles with decreasing diameter could cause the growth to fail, by reducing the driving force for the transport of Sb from the vapor to the particle (effective supersaturation). To focus the analysis on the nucleation event, we measured the smallest stem diameter with successful GaSb growth for each sample in the precursor partial pressures series (series A), as illustrated in Figure 3c. To analyze these critical diameters we use the expression for the growth rate of nanowires affected by surface diffusion and the Gibbs–Thomson effect derived in ref 32 and used in refs 33 and 11 (see Materials and Methods section for details). Solving for the critical diameter, d_{crit} where no growth occurs, yields

$$d_{\text{crit}} = \frac{4\gamma_a \Omega_a}{k_B T \ln \left(\frac{\alpha p_{\text{TMSb}}}{x p_v^*} \right)}$$

where γ_a and Ω_a are, respectively, the surface energy and the atomic volume of the alloy particle, α is the utilization factor for the Sb precursor, p_v^* is the saturation vapor pressure of pure Sb, and x is the steady-state Sb fraction in the alloy particle during growth. It is reasonable to assume that the Sb fraction should increase with increasing TMSb partial pressure (that is, supersaturation in the alloy is connected to the vapor supersaturation). As a first approximation we use a linear model

$$x(p_{\text{TMSb}}) = x_{\text{eq}} + k \times p_{\text{TMSb}}$$

where the steady-state Sb fraction increases from the equilibrium Sb fraction, x_{eq} , proportionally to the TMSb pressure by a factor k . We obtained the best fit for our data with $x_{\text{eq}} = 0.005$, $k = 0.12 \text{ Pa}^{-1}$ and $\alpha = 0.075$. For the lowest p_{TMSb} of 0.096 Pa GaSb did not nucleate on any of the nanowires, and this point could therefore not be directly used for fitting the model. However, it

serves as a check for the validity of the model's predictions.

Although the model was fitted to only three measurements we note that it is consistent with several more aspects of our growths. The critical diameter is predicted to increase dramatically at low TMSb pressures and no growth should occur at $p_{\text{TMSb}} < 0.1 \text{ Pa}$ for any diameter, which is verified by the failed growths for the $p_{\text{TMSb}} = 0.096 \text{ Pa}$ sample. Additionally, the Sb fraction in the alloy particle should increase with p_{TMSb} according to the model, but still be in the range of only a few atom % (e.g., with a predicted Sb fraction of 0.05 during growth for $p_{\text{TMSb}} = 0.380$). EDX measurements postgrowth do show an increase of the Sb fraction in the catalyst with increasing p_{TMSb} used during growth; a small but statistically significant difference of $x = 0.013$ and 0.021 was found for growths using $p_{\text{TMSb}} = 0.285$ and 0.380 Pa , respectively, ($p = 0.0002$ in a one-tailed test).

In the above analysis we have used the material-related parameters for pure gold and have fitted the remaining unknown parameters (utilization factor α and Sb fraction x) to the measured critical diameters. As the alloy particles in III–Sb growth usually contain more group III atoms than Au atoms, one would expect a material-dependent difference in these parameters compared to pure gold. When a single materials system is analyzed the differences in the material related parameters from pure gold is however compensated by the fitted parameters. This allowed us to make quantitative predictions within the InAs–GaSb system. Qualitatively, the behavior observed here should also be relevant for other related systems, which could be investigated using the same principles. One could speculate that the Gibbs–Thomson diameter limit is larger or smaller in other materials systems due to differences in the material-related parameters, but this effect would be complicated to disentangle from the simultaneous changes in utilization factor or relation between TMSb pressure and Sb fraction in the alloy particle. The model also suggests that the choice of catalyst material could affect the diameter limit. A lower atomic volume or surface energy would for instance be beneficial, as would a lower solubility of the growth species. For III–Sb materials both In (i.e., self-seeded growth)^{5,6} and Ag⁹ has proven to yield epitaxial nanowires, but not thin enough that any difference to Au in this regard can be evaluated.

Further Reductions in Diameter. To decrease the critical diameter even further, and enable growth of even thinner GaSb, the model together with the growth series presents two possibilities: further increasing either the GaSb growth temperature or the precursor partial pressures. The GaSb growth temperature can however not be increased further as the InAs stems, especially the thinner ones, will decompose due to the

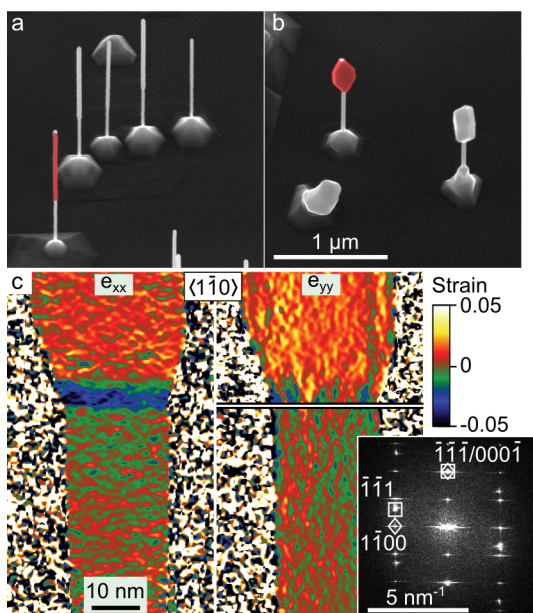


Figure 4. (a–b) SEM images recorded at 30° tilt from samples grown with $p_{\text{TMSb}} = 0.543$ Pa at $\text{V}/\text{III} = 1.5$ for 20 and 30 nm particles, respectively (sample E). A large number of the nanowires in panel a contain a GaSb segment (marked red for one nanowire in each sample), which is also the case in image b. However, for the larger diameters significant overgrowth occurs and the resulting structures have a drastically reduced aspect ratio. (c) Strain maps from a nanowire with a stem diameter of 21 nm, calculated from a HRTEM image recorded in a $\langle 1-10 \rangle$ projection. The reduced (111) plane distance at the interface between the InAs and GaSb segments indicates the presence of an approximately 9 nm long transition region. The inset shows the diffractogram of the same nanowire and indicates which reflections were used to produce the strain maps for the zincblende (□) and wurtzite (◊) segments.

As-deficient environment during GaSb growth. For the precursor partial pressures the model indicates that there is some room for further decreasing the diameter of the GaSb segment by further increasing the TMSb partial pressure, but that increasing partial pressures will eventually give diminishing returns. Figure 3c shows the critical diameter approaching 22 nm asymptotically, allowing a potential diameter reduction of only a few more nanometers. In practice the limit may be somewhat higher as the mass flow controllers in the MOVPE system always put an upper limit to the flows.

However, the results of series C shown in Figure 1c suggest that the V/III ratio may play a role in the yield in addition to the absolute magnitude of the TMSb flow. The flow of TMGa may affect the Sb supersaturation either directly (if the precursors decompose competitively, as suggested in ref 11) or indirectly (if the species form a nonideal solution with gold, their respective chemical potentials will be interrelated). To test this we attempted to grow nanowires from nominally 20 and 30 nm gold particles by increasing the TMSb partial pressure from the reference conditions to 0.543 Pa (sample E), thereby also increasing the V/III to 1.5. SEM images of the resulting structures are shown in Figure 4

panels a and b, respectively. It can immediately be seen that at least some of the nanowires grown from 20 nm gold particles show the same type of diameter increase as the successful InAs–GaSb nanowires in Figure 1c, indicating that a GaSb segment has been formed with an overall yield of 65%. This was confirmed using TEM and EDX, where we observed GaSb segments for InAs stem diameter as small as 21 nm. To illustrate the compositional profile in the interface region, a map of the local lattice parameter is shown in Figure 4c, measured both parallel and perpendicular to the growth direction. This map, containing a 9 nm transition region between the InAs and GaSb segments, was calculated using the geometrical phase analysis method. The contraction of the (111) planes perpendicular to the growth direction indicates $\text{In}_{0.5}\text{Ga}_{0.5}\text{As}$, which matches well the previous growths. The diameter of the GaSb segment is here only 32 nm, which is the smallest diameter reported thus far for GaSb nanowires grown by MOVPE.

The nanowires grown from 30 nm particles with the higher p_{TMSb} also show two distinct segments, though the GaSb segment is heavily overgrown and has lost the high aspect ratio which was obtained for the 20 nm gold particles (or from larger particles at lower p_{TMSb}). In this case the resulting GaSb segment is increasingly dominated, compared to the growth direction, by the inclined $\{111\}$ facets rather than the parallel $\{110\}$ facets which normally bound the GaSb nanowires. Similar results have also been observed for InSb⁷ and GaInSb,¹¹ where the nanowires eventually transitioned to nanodiamonds bound almost entirely by $\{111\}$ facets. This highlights the need to optimize the flows for the desired diameter of the InAs–GaSb: high flows are needed in order to nucleate and grow high aspect ratio GaSb segments for small particle diameters but if set too high will instead result in high radial overgrowth and a decreased aspect ratio. As diameter decreases, this optimization becomes increasingly important.

CONCLUSIONS

The growth of GaSb on InAs stems is highly sensitive to the precursor partial pressures (more specifically the TMSb partial pressure), which can be seen by the sharp decrease in yield when these are reduced below some threshold value. We found that the yield was also diameter dependent, as no GaSb segment nucleated on nanowires with InAs stems thinner than a certain critical diameter. This critical diameter is in turn dependent on the precursor partial pressures and could be decreased, thus enabling the growth of thinner InAs–GaSb nanowires, by increasing the precursor partial pressures. We suggest that these results can be explained by a Gibbs–Thomson model where the Sb supersaturation in the alloy particle is reduced due to the high Sb vapor pressure in small diameter particles. This model predicts that further increasing

the precursor partial pressures allows for further diameter reductions, but will eventually give diminishing returns. A further increase in TMSb partial pressure was attempted, and resulted in successful growth from 21 nm stems, producing 32 nm GaSb. However the very high precursor partial pressures used in this case resulted in increased overgrowth and reduced aspect

ratio for nanowires grown from larger diameter particles under these conditions. In summary, this study shows that as the diameter decreases below 30 nm it will become increasingly important to optimize (rather than maximize) the Sb partial pressure in order to overcome the Gibbs–Thomson effect without increasing the radial growth.

MATERIALS AND METHODS

Epitaxial Growth. Gold aerosol nanoparticles with diameters of 30–70 nm were deposited on epi-ready InAs(111)B substrates at an average surface concentration of $1 \mu\text{m}^{-2}$. The nanowire heterostructures were epitaxially grown on these substrates by MOVPE using trimethylgallium (TMGa), trimethylindium (TMIIn), trimethylantimony (TMSb), and arsine (AsH_3) as precursors. The following procedure was used to grow the InAs–GaSb sample used as a reference throughout this report: first the sample was heated under 15 Pa AsH_3 at 550 °C, at a reactor total pressure of 10 kPa and 13 L/min flow. The temperature was then lowered to 450 °C and InAs growth was commenced by introducing 0.045 Pa TMIIn and reducing the AsH_3 partial pressure to 1.9 Pa. To switch to GaSb growth TMIIn was turned off, AsH_3 was increased to 15 Pa, and the temperature was ramped to the GaSb growth temperature ($T_{\text{GaSb}} = 500$ °C) over 1 min. When the desired growth temperature was reached, AsH_3 was turned off and TMGa and TMSb turned on (0.36 and 0.38 Pa, respectively, giving a V/III of 1.1). Normally GaSb was grown for 30–45 min, but to characterize the difference between successful and failed nanowires closely after the GaSb nucleation, the growth was terminated after only 5 min for one sample.

This procedure was modified in four series to determine the requisite conditions for nucleating the GaSb segment on the InAs stem. In the first series (series A) the precursor partial pressures were modified by setting $p_{\text{TMSb}} = 0.095, 0.190, 0.285$, and 0.380 Pa at a constant V/III of 1.1 (the last sample following the reference procedure). In a second series (series B) the growth temperature of the GaSb segment was modified to $T_{\text{GaSb}} = 450, 465, 485, 500$, and 520 °C while otherwise following the reference procedure. For both series GaSb was grown for 30 min. Series C consisted of two samples with differing V/III ratios of 0.54 and 2.1 using $p_{\text{TMSb}}/p_{\text{TMGa}}$ of 0.190/0.355 and 0.380/0.177 Pa, respectively, all grown at $T_{\text{GaSb}} = 500$ °C to be comparable with the reference procedure. In the fourth series (series D) the growth time, and hence the length, of the InAs stem was varied between 7 and 13 min while otherwise following the reference procedure.

Following the analysis of these growths with the Gibbs–Thomson model we attempted to grow the InAs–GaSb structure from even smaller gold particles (sample E). For this growth, 20 nm gold particles (as well as 30–70 nm) were used at a growth temperature of 500 °C, $p_{\text{TMSb}} = 0.543$ and V/III = 1.5.

Gibbs–Thomson Model. For studying the influence of the Gibbs–Thomson effect we adapt the model derived in ref 32 and previously used in refs 11 and 33. From this expression we evaluate the critical radius below which no growth can occur by setting the growth rate $dL/dt = 0$. This is equivalent to

$$0 = \alpha p_{\text{TMSb}} - p_v$$

where α denotes the utilization factor of TMSb, p_{TMSb} is the TMSb partial pressure in the reactor, and p_v is the Sb vapor pressure in the alloy particle. As the steady state fraction of Sb in the gold particle, x , is low we assume that Raoult's law applies. By including the Gibbs–Thomson effect p_v can now be expressed as

$$p_v = x p_v^* \exp\left(\frac{2\gamma_a \Omega_a}{r k_B T}\right)$$

where p_v^* is the saturation vapor pressure of pure Sb, and γ_a and Ω_a are the surface energy and the atomic volume of the alloy particle, respectively. As a first approximation we use the values for gold ($\gamma = 1.2 \text{ J/m}^2$ and $\Omega = 10.2 \times 10^{-6} \text{ m}^3/\text{mol}$). We also assume a simple model to describe the relationship between x and p_{TMSb} , where x increases linearly with p_{TMSb} from some equilibrium value x_{eq} . These equations can now be solved for r to yield the result described in the main text.

SEM Characterization. Scanning electron microscopy (SEM) was used to investigate the resulting heterostructures (LEO 1560 operated at 15 kV). In each sample the nanowires were grouped by the diameter of their InAs stems, including any GaSb shell, into 5 nm cohorts with $d_{\text{stem}} \pm 2.5 \text{ nm}$. The yield of GaSb segments (visible due to the associated diameter increase) was evaluated for each cohort. Because of the change of side facets from {1100} in the wurtzite InAs to {110} in the zincblende GaSb, the two segments have the shape of hexagonal prisms rotated 60° with respect to one another, which should be taken into account when measuring diameters.³⁴ In our case the InAs becomes rounded during the GaSb growth, mainly because of etching due to the As deficient conditions, which makes the viewing direction less important. In all cases for GaSb the diameter is here reported as the diameter of the circle in which the hexagonal cross-section of the segment can be inscribed.

TEM Characterization. Samples for TEM characterization were prepared by gently pressing a lacey carbon Cu grid to the substrate. High resolution TEM (HRTEM) and scanning TEM (STEM) together with energy dispersive X-ray spectroscopy (EDX) was used for structural and compositional characterization, respectively. The EDX maps used for calculating compositional profiles across the heterojunctions were noise filtered by a principal component analysis method.³⁷ These profiles were in turn quantified under the assumption that the V/III ratio in the solid material is 1, using reference spectra from the pure binary materials. For the thinnest nanowires, where EDX produced insufficient signal, the composition was estimated from the local lattice parameter which was measured using the geometric phase analysis (GPA) method.³⁸ All TEM analysis was performed on a 300 kV JEOL 3000F microscope.

Conflict of Interest: The authors declare no competing financial interests.

Acknowledgment. This work was supported by the Swedish Research Council (VR), the Swedish Foundation for Strategic Research (SSF), VINNOVA, the Knut and Alice Wallenberg Foundation (KAW), and by the Nanometer Structure Consortium at Lund University (nmC@LU). The authors thank L.-E. Wernersson, C. Thelander, B. Ganjipour, and A.W. Dey for helpful discussions and support during the course of this project.

REFERENCES AND NOTES

- Guo, Y. N.; Zou, J.; Paladugu, M.; Wang, H.; Gao, Q.; Tan, H. H.; Jagadish, C. Structural Characteristics of GaSb/GaAs Nanowire Heterostructures Grown by Metal–Organic Chemical Vapor Deposition. *Appl. Phys. Lett.* **2006**, *89*, 231917.
- Jeppsson, M.; Dick, K. A.; Wagner, J. B.; Caroff, P.; Deppert, K.; Samuelson, L.; Wernersson, L. GaAs/GaSb Nanowire Heterostructures Grown by MOVPE. *J. Cryst. Growth* **2008**, *310*, 4115–4121.

3. Burke, R. A.; Weng, X.; Kuo, M.-W.; Song, Y.-W.; Itsuno, A. M.; Mayer, T. S.; Durbin, S. M.; Reeves, R. J.; Redwing, J. M. Growth and Characterization of Unintentionally Doped GaSb Nanowires. *J. Electron. Mater.* **2010**, *39*, 355–364.
4. Caroff, P.; Messing, M. E.; Borg, B. M.; Dick, K. A.; Deppert, K.; Wernersson, L.-E. InSb Heterostructure Nanowires: MOVPE Growth under Extreme Lattice Mismatch. *Nanotechnology* **2009**, *20*, 495606.
5. Pozuelo, M.; Zhou, H.; Lin, S.; Lipman, S. A.; Goorsky, M. S.; Hicks, R. F.; Kodambaka, S. Self-Catalyzed Growth of InP/InSb Axial Nanowire Heterostructures. *J. Cryst. Growth* **2011**, *329*, 6–11.
6. Mandl, B.; Dick, K. A.; Kriegner, D.; Keplinger, M.; Bauer, G.; Stangl, J.; Deppert, K. Crystal Structure Control in Au-free Self-Seeded InSb Wire Growth. *Nanotechnology* **2011**, *22*, 145603.
7. Plissard, S. R.; Slapak, D. R.; Verheijen, M. A.; Hocevar, M.; Immink, G. W. G.; van Weperen, I.; Nadj-Perge, S.; Frolov, S. M.; Kouwenhoven, L. P.; Bakkers, E. P. A. M. From InSb Nanowires to Nanocubes: Looking for the Sweet Spot. *Nano Lett.* **2012**, *12*, 1794–1798.
8. Ercolani, D.; Rossi, F.; Li, A.; Roddaro, S.; Grillo, V.; Salvati, G.; Beltram, F.; Sorba, L. InAs/InSb Nanowire Heterostructures Grown by Chemical Beam Epitaxy. *Nanotechnology* **2009**, *20*, 505605.
9. Vogel, A. T.; de Boor, J.; Wittemann, J. V.; Mensah, S. L.; Werner, P.; Schmidt, V. Fabrication of High-Quality InSb Nanowire Arrays by Chemical Beam Epitaxy. *Cryst. Growth Des.* **2011**, *11*, 1896–1900.
10. Xu, T.; Dick, K. A.; Plissard, S. R.; Nguyen, T. H.; Makoudi, Y.; Berthe, M.; Nys, J.-P.; Wallart, X.; Grandidier, B.; Caroff, P. Faceting, Composition and Crystal Phase Evolution in III–V Antimonide Nanowire Heterostructures Revealed by Combining Microscopy Techniques. *Nanotechnology* **2012**, *23*, 095702.
11. Ghahamestani, S. G.; Ek, M.; Ganjipour, B.; Thelander, C.; Johansson, J.; Caroff, P.; Dick, K. A. Demonstration of Defect-Free and Composition Tunable Ga_xIn_{1-x}Sb Nanowires. *Nano Lett.* **2012**, *12*, 4914–4919.
12. Dheeraj, D. L.; Patriarche, G.; Largeau, L.; Zhou, H. L.; van Helvoort, A. T. J.; Glas, F.; Harmand, J. C.; Fimland, B.-O.; Weman, H. Zinc Blende GaAsSb Nanowires Grown by Molecular Beam Epitaxy. *Nanotechnology* **2008**, *19*, 275605.
13. Plissard, S. R.; Dick, K. A.; Wallart, X.; Caroff, P. Gold-free GaAs/GaAsSb Heterostructure Nanowires Grown on Silicon. *Appl. Phys. Lett.* **2010**, *96*, 121901.
14. Borg, B. M.; Dick, K. A.; Eymery, J.; Wernersson, L.-E. Enhanced Sb Incorporation in InAsSb Nanowires Grown by Metalorganic Vapor Phase Epitaxy. *Appl. Phys. Lett.* **2011**, *98*, 113104.
15. Ercolani, D.; Gemmi, M.; Nasi, L.; Rossi, F.; Pea, M.; Li, A.; Salvati, G.; Beltram, F.; Sorba, L. Growth of InAs/InAsSb Heterostructured Nanowires. *Nanotechnology* **2012**, *23*, 115606.
16. Zhou, H.; Pozuelo, M.; Hicks, R. F.; Kodambaka, S. Self-Catalyzed Vapor–Liquid–Solid Growth of InP_{1-x}Sb_x Nanostructures. *J. Cryst. Growth* **2011**, *319*, 25–30.
17. Glas, F. Critical Dimensions for the Plastic Relaxation of Strained Axial Heterostructures in Free-Standing Nanowires. *Phys. Rev. B* **2006**, *74*, 121302(R).
18. Mourik, V.; Zuo, K.; Frolov, S. M.; Plissard, S. R.; Bakkers, E. P. A. M.; Kouwenhoven, L. P. Signatures of Majorana Fermions in Hybrid Superconductor–Semiconductor Nanowire Devices. *Science* **2012**, *336*, 1003–1007.
19. Deng, M. T.; Yu, C. L.; Huang, G. Y.; Larsson, M.; Caroff, P.; Xu, H. Q. Anomalous Zero-Bias Conductance Peak in a Nb–InSb Nanowire–Nb Hybrid Device. *Nano Lett.* **2012**, *12*, 6414–6419.
20. Koswatta, S. O.; Koester, S. J.; Haensch, W. On the Possibility of Obtaining MOSFET-like Performance and Sub-60-mV/dec Swing in 1-D Broken-Gap Tunnel Transistors. *IEEE Trans. Electron Devices* **2010**, *57*, 3222–3230.
21. Dey, A. W.; Borg, B. M.; Ganjipour, B.; Ek, M.; Dick, K. A.; Lind, E.; Thelander, C.; Wernersson, L.-E. High-Current GaSb/InAs (Sb) Nanowire Tunnel Field-Effect Transistors. *IEEE Electron Device Lett.* **2013**, *34*, 211–213.
22. Ganjipour, B.; Nilsson, H. A.; Mattias Borg, B.; Wernersson, L.-E.; Samuelson, L.; Xu, H. Q.; Thelander, C. GaSb Nanowire Single-Hole Transistor. *Appl. Phys. Lett.* **2011**, *99*, 262104.
23. Yang, X.; Wang, G.; Slattery, P.; Zhang, J. Z.; Li, Y. Ultrasmall Single-Crystalline Indium Antimonide Nanowires. *Cryst. Growth Des.* **2010**, *10*, 2479–2482.
24. Paul, R. K.; Penchev, M.; Zhong, J.; Ozkan, M.; Ghazinejad, M.; Jing, X.; Yengel, E.; Ozkan, C. S. Chemical Vapor Deposition and Electrical Characterization of Sub-10 nm Diameter InSb Nanowires and Field-Effect Transistors. *Mater. Chem. Phys.* **2010**, *121*, 397–401.
25. Vaddiraju, S.; Sunkara, M. K.; Chin, A. H.; Ning, C. Z.; Dholakia, G. R.; Meyyappan, M. Synthesis of Group III Antimonide Nanowires. *J. Phys. Chem. C* **2007**, *111*, 7339–7347.
26. Park, H. D.; Prokes, S. M.; Twigg, M. E.; Ding, Y.; Wang, Z. L. Growth of High Quality, Epitaxial InSb Nanowires. *J. Cryst. Growth* **2007**, *304*, 399–401.
27. Zi, Y.; Zhao, Y.; Candebat, D.; Appenzeller, J.; Yang, C. Synthesis of Antimony-Based Nanowires Using the Simple Vapor Deposition Method. *ChemPhysChem* **2012**, *13*, 2585–2588.
28. Lugani, L.; Ercolani, D.; Sorba, L.; Sibirev, N. V.; Timofeeva, M. A.; Dubrovskii, V. G. Modeling of InAs–InSb Nanowires Grown by Au-Assisted Chemical Beam Epitaxy. *Nanotechnology* **2012**, *23*, 095602.
29. Ganjipour, B.; Dey, A. W.; Borg, B. M.; Ek, M.; Pistol, M.-E.; Dick, K. A.; Wernersson, L.-E.; Thelander, C. High Current Density Esaki Tunnel Diodes Based on GaSb–InAsSb Heterostructure Nanowires. *Nano Lett.* **2011**, *11*, 4222–4226.
30. Ek, M.; Borg, B. M.; Dey, A. W.; Ganjipour, B.; Thelander, C.; Wernersson, L.-E.; Dick, K. A. Formation of the Axial Heterojunction in GaSb/InAs(Sb) Nanowires with High Crystal Quality. *Cryst. Growth Des.* **2011**, *11*, 4588–4593.
31. Borg, B. M.; Dick, K. A.; Ganjipour, B.; Pistol, M.-E.; Wernersson, L.-E.; Thelander, C. InAs/GaSb Heterostructure Nanowires for Tunnel Field-Effect Transistors. *Nano Lett.* **2010**, *10*, 4080–4085.
32. Johansson, J.; Svensson, C. P. T.; Mårtensson, T.; Samuelson, L.; Seifert, W. Mass Transport Model for Semiconductor Nanowire Growth. *J. Phys. Chem. B* **2005**, *109*, 13567–13571.
33. Fröberg, L. E.; Seifert, W.; Johansson, J. Diameter-Dependent Growth Rate of InAs Nanowires. *Phys. Rev. B* **2007**, *76*, 153401.
34. Lugani, L.; Ercolani, D.; Rossi, F.; Salvati, G.; Beltram, F.; Sorba, L. Faceting of InAs–InSb Heterostructured Nanowires. *Cryst. Growth Des.* **2010**, *10*, 4038–4042.
35. Larsson, M. W.; Wagner, J. B.; Wallin, M.; Håkansson, P.; Fröberg, L. E.; Samuelson, L.; Wallenberg, L. R. Strain Mapping in Free-Standing Heterostructured Wurtzite InAs/InP Nanowires. *Nanotechnology* **2007**, *18*, 015504.
36. Rathi, M. K.; Hawkins, B. E.; Kuech, T. F. Growth Behavior of GaSb by Metal–Organic Vapor-Phase Epitaxy. *J. Cryst. Growth* **2006**, *296*, 117–128.
37. Burke, M. G.; Watanabe, M.; Williams, D. B.; Hyde, J. M. Quantitative Characterization of Nanoprecipitates in Irradiated Low-Alloy Steels: Advances in the Application of FEG-STEM Quantitative Microanalysis to Real Materials. *J. Mater. Sci.* **2006**, *41*, 4512–4522.
38. Hytch, M. J.; Snoeck, E.; Kilaas, R. Quantitative Measurement of Displacement and Strain Fields from HREM Micrographs. *Ultramicroscopy* **1998**, *74*, 131–146.